ACS APPLIED ENERGY MATERIALS

www.acsaem.org Article

Facile and Low-Cost Fabrication of Cu/Zn/Sn-Based Ternary and Quaternary Chalcogenides Thermoelectric Generators

Ubaidah Syafiq,* Eleonora Isotta, Narges Ataollahi, Ketan Lohani, Sally Luong, Vanira Trifiletti, Oliver Fenwick, and Paolo Scardi*

Cite This: *ACS Appl. Energy Mater.* 2022, 5, 5909−5918 Read Online

ACCESS | Metrics & More | Article Recommendations | Supporting Information

ABSTRACT: In this work, Cu/Zn/Sn-based ternary and quaternary chalcogenides inks were synthesized via hot injection and/or from ball-milled powders. The synthesized inks were used to fabricate thermoelectric generators (TEGs) based on *p*-type chalcogenide and *n*-type aluminum-doped zinc oxide (AZO) thin films via spin-coating and magnetron sputtering, respectively. This work highlights the first-ever attempt in a facile and scalable method to fabricate thin-film TEGs using safe, low-cost, and abundant materials. Four different TEGs were fabricated using Cu_2ZnSnS_4 (CZTS), $Cu_2ZnSnSe_4$ (CZTSe), $Cu_{2.125}Zn_{0.875}SnS_3Se$ (CZTSSe), and Cu_2SnS_3 (CTS) chalcogenides. Thermoelectric transport analysis confirmed the respective *p*- and *n*-type natures of the chalcogenides and AZO, with their Seebeck coefficients compatible to be coupled in a *p*−*n* device. In addition, a full-device analysis has been carried out, and several factors affecting the performance of TEGs were investigated, including the composition, density, and presence of secondary phases in chalcogenide thin films. The maximum power per unit active planar area obtained for CZTS, CZTSe, CZTSSe, and CTS TEGs at a temperature difference (ΔT) of 160 K was ∼43, ∼188, ∼23, and ∼59 nW/cm^2, respectively, making CZTSe/AZO TEG the champion device.

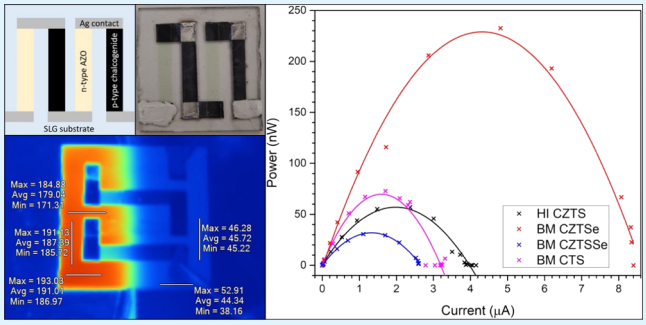

KEYWORDS: *thermoelectric generator (TEG), thin film, $Cu_2ZnSn(S/Se)_4$ (CZTS/Se), Cu_2SnS_3 (CTS), aluminium-doped zinc oxide (AZO)*

Downloaded via 34.98.143.3 on April 1, 2024 at 19:35:06 (UTC).
See https://pubs.acs.org/sharingguidelines for options on how to legitimately share published articles.

1. INTRODUCTION

A thermoelectric generator (TEG) is a solid-state device that converts thermal energy into electrical energy and vice versa through the Seebeck effect.[1] TEGs possess attractive features for renewable energy applications, as they are characterized by no moving parts, no emissions of toxic gases, a long life span, low maintenance needs, and high reliability.[2] A TEG basic unit consists of a pair of thermoelements (*p*- and *n*-type semiconducting materials) connected electrically in series by a conducting strip and thermally in parallel. These units are used as building blocks for the construction of a TEG module.

Nowadays, thermoelectricity has been studied and applied in a wider range of applications including medical applications,[3] coolers,[4] and temperature sensors.[5] Even though the development of TEG technologies has vastly improved in recent decades, wide commercialization is still limited, mainly due to the complexity of integration, low efficiencies, and high cost of fabricating high-performance TEGs, which are usually made of alloys of expensive and rare-earth materials such as tellurium (Te) and bismuth (Bi).[6] Thus, any efforts in fabricating low-cost TEGs with decent performance may push the development of this technology toward commercialization.

Thickness reduction is an option to fabricate low-cost TEGs with improved performance. Indeed, a thin-film configuration favors a number of mechanisms that can enhance thermoelectric transport properties such as low-dimensional quantum confinement and reduction of lattice thermal conductivity[7−9] through the well-known effect of interface scattering between the thin film and substrate or between multilayers.[6,10] This approach gave a new paradigm for TE materials to untangle the interrelated electrical and thermal properties.[11−13] Due to the reduction in thickness, TE materials offer additional opportunities in microdevices such as micro-TEGs,[14,15] microcoolers,[4,16] and microsensors.[17]

Materials for TEG application can be divided into three classes based on their optimum working temperature ranges; low temperature (up to 450 K), middle temperature (up to 850 K) and high temperature (>850 K).[18] Several materials

Received: January 24, 2022
Accepted: March 10, 2022
Published: April 19, 2022

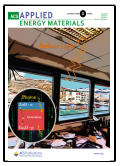

© 2022 The Authors. Published by American Chemical Society

have been explored to fabricate these devices, including semiconductors,[6,19] fibers,[20] and conducting polymers.[21] In recent years, chalcogenide semiconductors such as lead telluride (PbTe)[22] and bismuth telluride (Bi_2Te_3)[23] have been investigated for TE applications owing to their high power factors (PFs) due to the weaker covalent bonds on account of low electronegativity, along with the heavy atomic weights, which are beneficial in reducing thermal conductivity.[24] Unfortunately, due to their composition of mostly toxic and scarce elements, the attention diverted toward more sustainable and abundant chalcogenides, such as tin selenide (SnSe),[25] copper zinc tin sulfide (Cu_2ZnSnS_4, CZTS),[26−30] and copper tin sulfide (Cu_2SnS_3, CTS).[31−33]

Among the aforementioned chalcogenides, bulk Cu_2ZnSnS_4 (CZTS) is considered a good candidate for a sustainable and "green" medium of high-temperature TE material owing to its abundance and nontoxicity of the constituent elements,[34] along with good physical, thermal, and chemical properties.[19,35] In general, quaternary chalcogenides like CZTS possess chemical and structural degrees of freedom, which offer flexibility in their physical properties.[36] In addition, by fully or partly replacing sulfur (S) with selenium (Se), CZTSe or CZTSSe can be produced. This replacement enables band gap tuning,[37] which makes it a versatile semiconducting material to be used in various applications. Despite the vast knowledge acquired in the past two decades on CZTS fabrication and properties,[38,39] thermoelectricity in CZTS thin films has been scarcely explored.[19] Several studies have been done in improving the thermoelectric properties of CZTS. Cation doping such as copper (Cu) doping[29,40] is proven as one of the efficacious strategies to enhance electrical conductivity and reduce thermal conductivity, which could be of benefit in improving the thermoelectric properties of CZTS.

CTS is another well-known, eco-friendly, nontoxic, and cost-effective *p*-type semiconducting material. CTS polymorphs are a variant of the zinc blende (ZnS) structure, made of tetrahedral cages of S-atoms with a Zn-atom positioned in the middle of the cage. In the ordered polymorph of CTS (space group: *Cc*), Zn is stoichiometrically replaced by Cu and Sn in an ordered manner. However, in the disordered polymorph of CTS (space group: $F\bar{4}3m$), the disorder takes the form of compositional inhomogeneities caused by entropy-driven clustering.[41] Disordered CTS shows a higher electrical conductivity, thanks to its lower band gap. More importantly, the disorder induced by the partial occupancy of cations helps in the suppression of the thermal conductivity to an ultralow level, presenting a ∼10-fold higher zT than that of its ordered counterpart.[32]

This study reports the synthesis of Cu/Zn/Sn-based ternary and quaternary chalcogenide inks including Cu_2ZnSnS_4 (CZTS), $Cu_2ZnSnSe_4$ (CZTSe), $Cu_{2.125}Zn_{0.875}SnS_3Se$ (CZTSSe), and Cu_2SnS_3 (CTS), using hot-injection synthesis or from ball-milled powders. The synthesized inks were then used to fabricate thin films, which were then coupled with aluminum-doped zinc oxide (AZO) thin films for the fabrication of TEGs. Currently available methods for the fabrication of thin-film TEGs such as pulsed laser deposition,[42] molecular beam epitaxy,[43] and magnetron sputtering[44] involve the use of specialized equipment or time-consuming processes.[45] This study demonstrates the potential of using a facile, low-cost, and scalable method to fabricate thin-film TEGs that are suitable for various applications.

Attempts at thin-film TEGs have mainly involved conventional thermoelectric materials such as PbTe[46] and Bi_2Te_3[8] in the past years. In addition, several attempts using more sustainable materials have also been reported for oxides and binary chalcogenides, such as SnSe[47] and aluminum oxide (Al_2O_3).[48] However, the class for ternary and quaternary Cu chalcogenides remains unexplored. To the best of our knowledge, this is a novel attempt at fabricating thin-film TEGs using *p*-type Cu/Zn/Sn-based chalcogenides. In addition, performance analyses of the fabricated TEGs were discussed, along with suggestions for further improvement and optimization.

2. MATERIALS AND METHODS

2.1. Synthesis of Cu/Zn/Sn-Based Chalcogenide Inks. Synthesis of CZTS nanoparticles via hot-injection synthesis was performed according to the method from some of the authors' previous work.[49] Meanwhile, CZTSe and CZTSSe ball-milled powders were synthesized via reactive mechanical alloying through a procedure similar to previous reports,[26,27] with the addition or substitution of Se using Se powder (Se, 99%, Alfa Aesar). CTS ball-milled powders were synthesized via reactive mechanical alloying of binary sulfides as previously reported.[31,33] The synthesized ball-milled powders were then used to obtain the respective chalcogenide inks. Details of the synthesis are provided in Supporting Information 1.

A particle analyzer (DelsaNano C, Beckman Coulter, Indianapolis) was used to measure the hydrodynamic size of ink particles. Details for DLS measurement are provided in Supporting Information 2. DLS analysis in Table 1 revealed that the synthesized ink particles had

Table 1. DLS Analysis of Synthesized Chalcogenide Inks

inks	particle preparation	average particle diameter (μm)
CZTS	hot-injection (HI)	0.020 ± 0.003
CZTSe	ball-milling (BM)	0.37 ± 0.01
CZTSSe	ball-milling (BM)	1.5 ± 0.4
CTS	ball-milling (BM)	3.7 ± 0.4

average diameters of ∼0.02, ∼0.37, ∼1.51, and ∼3.67 μm for CZTS, CZTSe, CZTSSe, and CTS, respectively. Ideally, an ink should have nanometric size particles for a stable dispersion. Unlike the hot-injection CZTS, OLA encapsulated the agglomerated nanodomains of the ball-milled chalcogenides,[26,27,31] causing the ink dispersions to consist of polycrystalline agglomerates that are micrometric in size.

Due to the micrometric size of particles in ball-milled (BM) chalcogenide inks, several challenges were faced during thin-film fabrication. Bigger size translates to heavier mass, which consequently increases the sedimentation rate of the agglomerates to the bottom of the ink, reducing the ink's stability. As a workaround, the inks were sonicated for several minutes right before deposition. In addition, the control of a film's thickness theoretically depends on the size of the polycrystalline agglomerates. Nevertheless, the synthesis of a more stable ink with smaller polycrystalline agglomerates is the subject of ongoing work.

2.2. Fabrication of Chalcogenides/AZO Thin-Film TEGs. Thin-film chalcogenides were deposited on soda-lime glass (SLG) substrates using a vacuum spin-coater (Laurell WS 650), followed by thermal treatment in a tube furnace (Carbolite CTF wire-wound) with a continuous flow of N_2.[50] Details of the fabrication is provided in Supporting Information 3. For the fabrication of chalcogenides/AZO thin-film TEGs (schematic is shown in Figure 1a), the device was designed to consist of two *p*-type chalcogenide legs and two *n*-type AZO legs arranged alternately and connected using a silver (Ag) metal contact in a zigzag pattern. Basically, the thermoelectric components are connected electrically in series and thermally in parallel. Kapton tape was used as the deposition mask on the SLG glass substrate and the *p*-legs were deposited by spin-coating, as

https://doi.org/10.1021/acsaem.2c00268
ACS Appl. Energy Mater. 2022, 5, 5909−5918

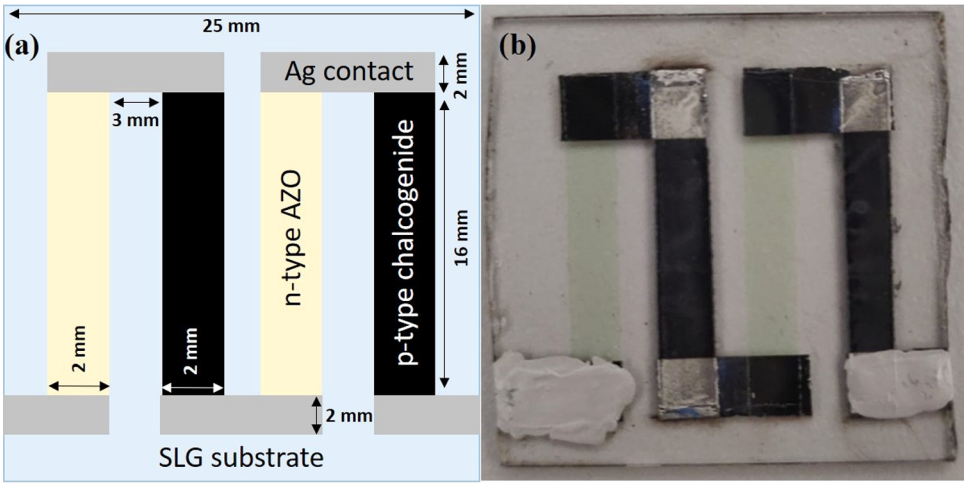

Figure 1. (a) Schematic design of a chalcogenide/AZO thin-film TEG (not drawn to scale) and (b) fabricated thin-film chalcogenide/AZO thin-film TEG.

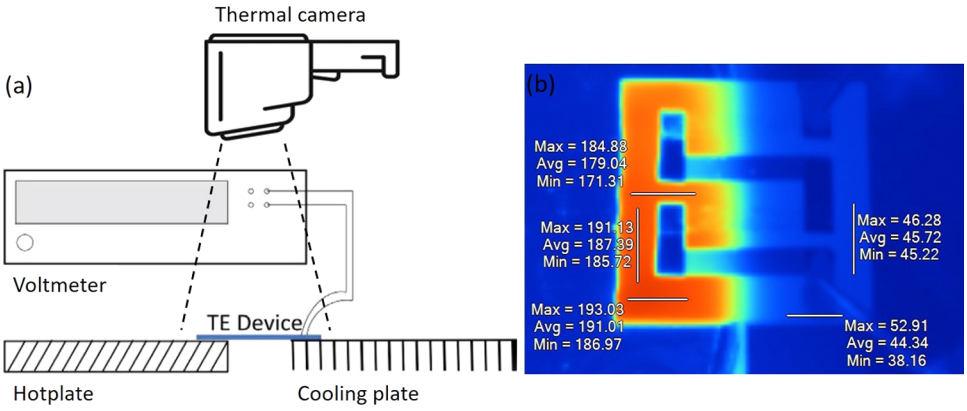

Figure 2. (a) Setup for V_{OC} vs ΔT measurement. (b) Thermal image of a chalcogenide/AZO thin-film TEG.

previously mentioned, while the *n*-legs were deposited using magnetron sputtering. Finally, Ag metal contacts were deposited via thermal evaporation. Figure 1b shows a fully fabricated thin-film chalcogenide/AZO thin-film TEG. Additional details regarding AZO and Ag deposition are provided in Supporting Information 4.

2.3. Performance Analysis of Chalcogenide/AZO Thin-Film TEG. The TEGs' internal resistances including each leg's resistance were measured using a handheld digital multimeter with a 200 mA/250 V fuse rating. Open-circuit voltage (V_{OC}) vs ΔT measurements were performed to evaluate the highest voltage that can be generated at varied temperature differences between the hot side (T_h) and the cold side (T_c) of the TEG. Figure 2a shows the setup used to conduct the V_{OC} vs ΔT measurements, where voltage measurements were taken from a Keithley 2601A multimeter while T_h and T_c were captured by a Fluke Ti25 Thermal Imager (Fluke Italia S.r.l., Brugherio, Italy) thermal camera. To avoid errors due to the differences in the emissivity of the materials, T_h and T_c values of the glass substrate were taken near the TEG legs as shown in Figure 2b. Validation for this assumption is discussed in Supporting Information 6.

I−*V*−*P* measurements were done to evaluate the performance of a TEG at specific temperature conditions (surrounding temperature, T_h, and T_c). The schematic of the *I*−*V*−*P* setup is presented in Figure 3a, while Figure 3b shows the homemade setup used. An ammeter (Hewlett-Packard 34401A multimeter) and a variable resistor were connected in series, while a voltmeter (Keithley 2601A multimeter) was connected in parallel with respect to the TEG. This measurement can be explained by a reduction in voltage when a current (I_2) is allowed by controlling R_C using the variable resistor. In an open

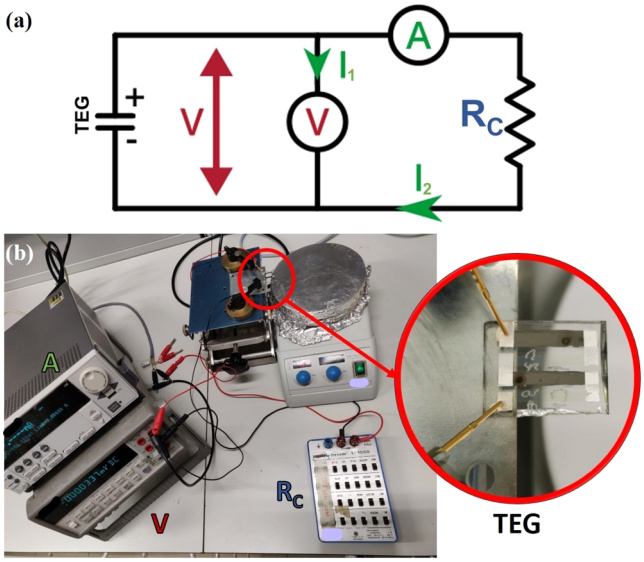

Figure 3. (a) Schematic setup for *I*−*V*−*P* measurement. (b) Picture of the in-house *I*−*V*−*P* measurement setup.

circuit, R_C is infinity, only I_1 current flows, and the TEG generates its highest voltage. However, there is no power output due to the zero current. By reducing R_C, the voltage decreases while I_2 increases. Upon reaching the short-circuit condition (zero R_C), I_2 reaches the

https://doi.org/10.1021/acsaem.2c00268
ACS Appl. Energy Mater. 2022, 5, 5909−5918

maximum value while voltage drops to zero. From the $I-V$ readings taken at varied R_C, the TEG's power curve can be calculated and plotted using $P = VI$.

3. RESULTS AND DISCUSSION

3.1. Characterization of Thin Films. The structural and compositional characterization of HI CZTS thin films including scanning electron microscopy (SEM), energy-dispersive X-ray spectrometry (EDXS), and X-ray diffraction (XRD) were investigated and reported in our previous paper.[19] Details for this discussion are provided in Supporting Information 7. As previously mentioned, the film thickness of fabricated Cu/Zn/Sn-based chalcogenides vary, mainly due to the size of the encapsulated particles in their inks. On average, HI CZTS possesses a thickness of ~2.0 μm, thanks to the nanometric size of particles in its ink. However, BM chalcogenide thin films suffer from poor thickness control due to the micrometric size of particles in their inks. The average thicknesses for BM CZTSe, BM CZTSSe, and BM CTS thin films were ~4.8, ~4.1, and ~5.1 μm, respectively (Figure S5, Supporting Information 8).

Table 2. EDXS Atomic Percentage for Each Element in the Fabricated AZO Thin Film

element	atomic percent (%)
Zn	35.9 ± 1.7
O	54.3 ± 2.7
Al	1.3 ± 1.3
Si	6.7 ± 0.2
Ca	1.8 ± 0.1

In addition, four-point probe resistance measurements on the films show that BM CTS possesses the lowest sheet resistance (0.87 ± 0.03 kΩ/□), followed by HI CZTS (1.6 ± 0.4 kΩ/□), BM CZTSe (5.0 ± 0.4 kΩ/□), and BM CZTSSe (5.6 ± 0.2 kΩ/□). HI CZTS thin film exhibits superior electrical properties owing to low sheet resistance and p-leg resistance as compared to BM chalcogenides due to its higher density. HI CZTS ink with lower particle size can better maximize the use of space during deposition, resulting in higher-density films. A film with a higher density exhibits better electrical properties since the pores in low-density films do not contribute to the material's electrical conductivity.[51] However, possibly due to the surface sensitivity of the four-point probes method, BM CTS presents the lowest sheet resistance, indicating that the film's surface might be continuous and connected.

For AZO thin film, SEM micrograph collected (Figure S6, Supporting Information 9) showed that the film covers the entirety of the substrate in a continuous and homogeneous manner. Some pinholes were observed, possibly due to the presence of contaminants during sputtering. EDXS analysis (Table 2) from the same SEM image revealed a high amount of Zn with some traces of Al with a compositional ratio of 27.6:1, which was close to the source composition. In addition, a higher atomic fraction of oxygen (O) than what was expected from AZO, along with trace amounts of silicon (Si) and

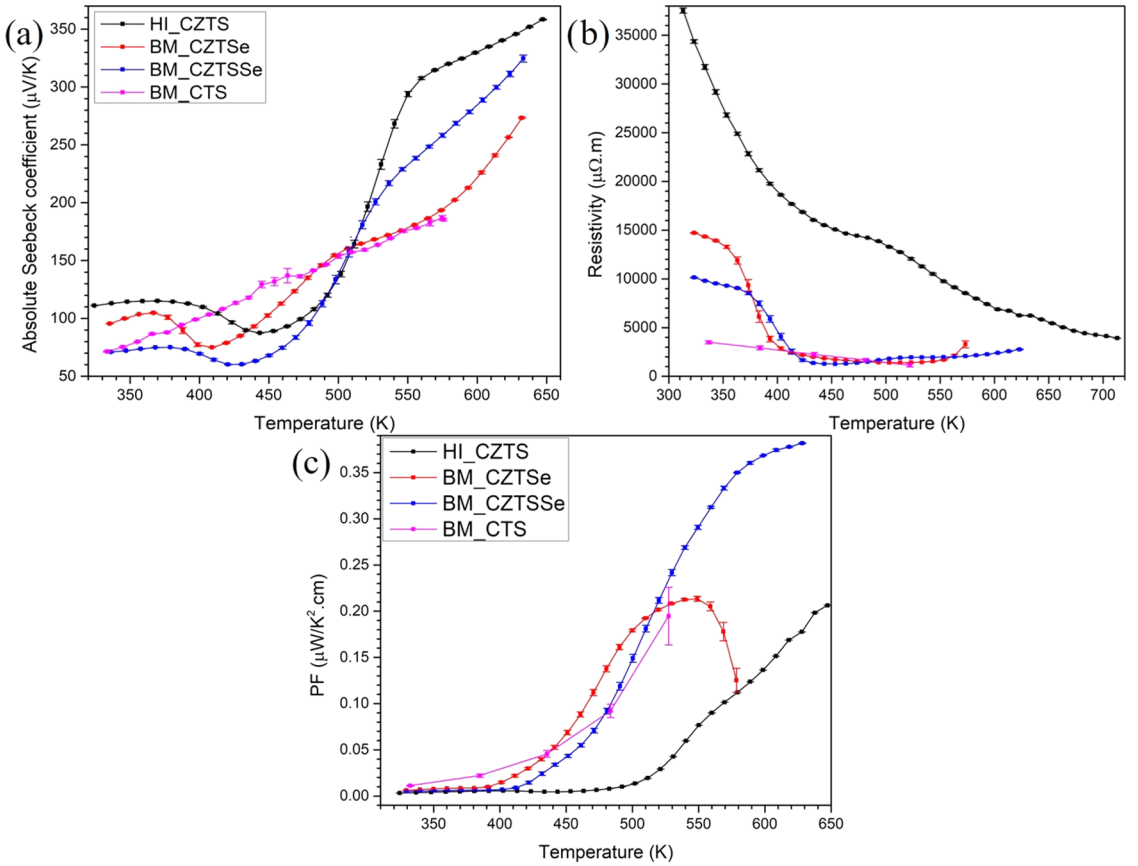

Figure 4. (a) Seebeck coefficient (α), (b) electrical resistivity (ρ), and (c) calculated power factor (PF) of HI CZTS, BM CZTSe, BM CZTSSe, and BM CTS thin films.

https://doi.org/10.1021/acsaem.2c00268
ACS Appl. Energy Mater. 2022, 5, 5909−5918

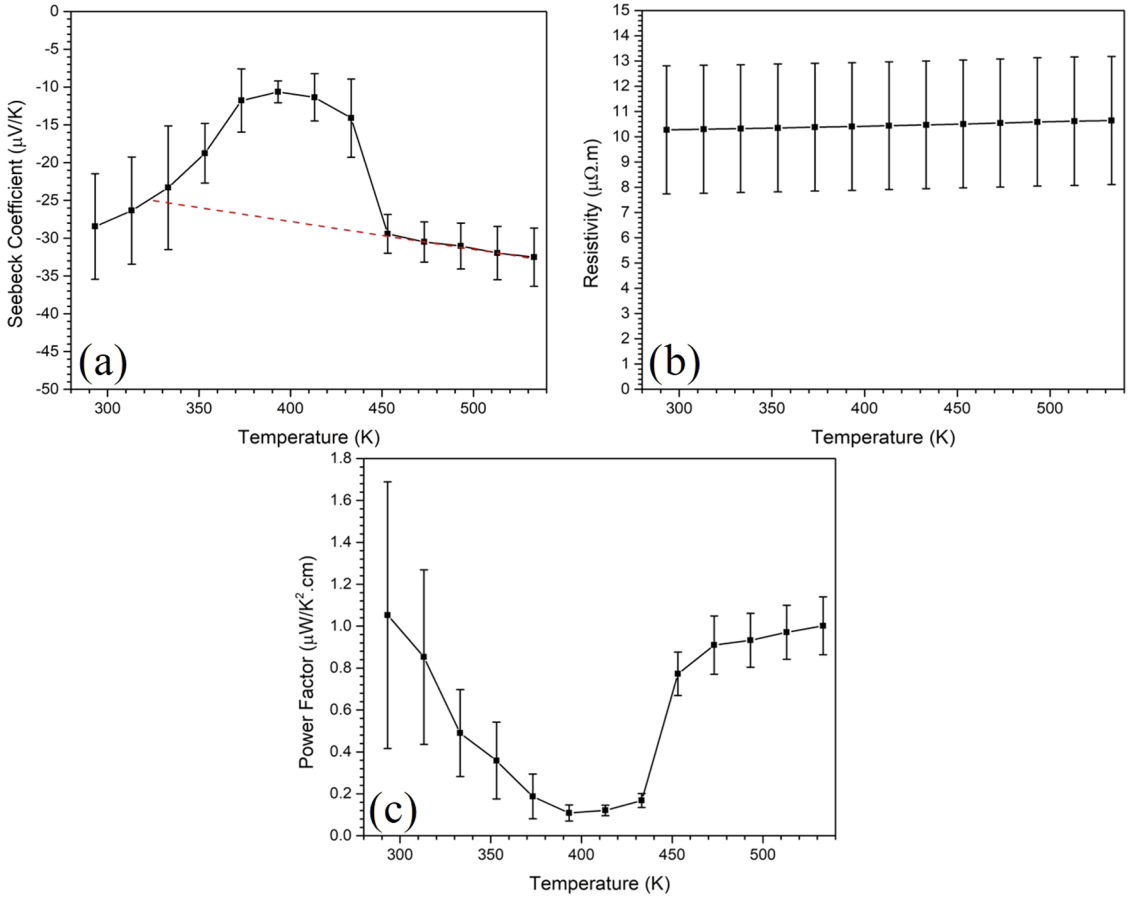

Figure 5. (a) α, (b) ρ, and (c) PF of the AZO thin film.

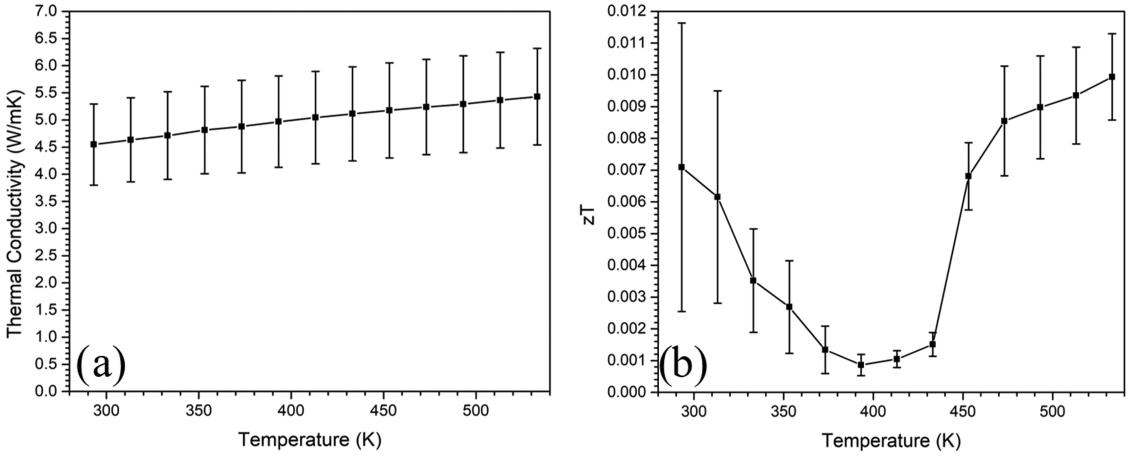

Figure 6. (a) Thermal conductivity (κ) and (b) zT of the AZO thin films.

calcium (Ca), was also observed, implying that the beam was able to penetrate through the deposited AZO layer to the substrate, preventing a precise determination of the sample stoichiometry.

The thickness of the AZO film was estimated to be 510 ± 50 nm using a surface profilometer. In addition, the XRD pattern (Figure S7, Supporting Information 9) showed that the fabricated AZO thin film possesses a ZnO-like zincite phase (PDF 00-005-0664). Only sharp Bragg peaks representing the (00l) planes were observed, confirming that the film was made of highly crystalline single-phase material, which had a preferred orientation along the [002] direction, with no observable peaks of spurious phases.

3.2. TE Transport Properties. The TE transport properties of the fabricated HI CZTS thin film are performed and reported thoroughly in our previous paper.[19] They are briefly discussed in Supporting Information 10. Nevertheless, Figure 4 shows α, ρ, and power factor (PF = α^2/ρ) of other fabricated Cu/Zn/Sn-based chalcogenide thin films, together with HI CZTS. The positive value of α for all chalcogenides indicates that holes are the major charge carriers, confirming the p-type conductivities.[31,49] The films generally exhibit low α and high ρ

https://doi.org/10.1021/acsaem.2c00268
ACS Appl. Energy Mater. 2022, 5, 5909−5918

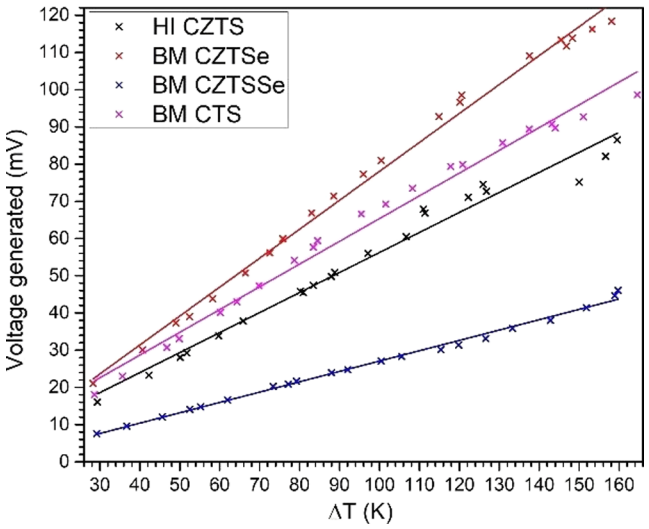

Figure 7. V_{OC} vs ΔT measurement of chalcogenides/AZO thin-film TEGs.

values in the low-temperature range, with a further increase in temperature increasing α and decreasing ρ. In addition, ρ presented a general decreasing trend, evidencing the non-degenerate semiconducting nature.[52] In addition, quaternary chalcogenides (CZTS, CZTSe, and CZTSSe) display a sharp rise in α at around 400−500 K, indicating the order−disorder transition from the ordered $I\bar{4}$ to disordered $I\bar{4}2m$ tetragonal structure[19,27,28] due to the randomization of Cu and Zn atoms among the 2*c* and 2*d* sites.[53] This phenomenon leads to a dramatic increase in the materials' PF, as is evident in Figure 4c.

On the other hand, TE transport properties of the AZO thin film were measured using Linseis Thin Film Analyser and reported in Figure 5a. The value of α was negative, indicating electrons as majority charge carriers.[54] An observation of the absolute value showed that α decreases with the temperature of up to ∼393 K. Further increase in temperature increased α, leading to a maximum value of ∼−33 μV/K at ∼533 K, in agreement with other reported values.[55] Overall, α measurement showed a linear trend, but with a slight deviation observed between ∼333 and ∼433 K.[56]

In addition, the electrical resistivity of the AZO thin film (Figure 5b) remains around ∼10 $\mu\Omega$·m up to ∼533 K, which is in accordance with other literature results.[55,57] The resistivity of AZO thin films shows a degenerate semiconductor nature, which increases with temperature, suggesting that AZO possesses a high-carrier concentration. From these two transport properties, the film's PF (Figure 5c) is calculated, which shows a decreasing trend with temperature up to ∼393 K, followed by an increase up to the maximum measured temperature. The variation of PF is mainly affected by the variation of α in temperature, as we observe limited variation in resistivity. The maximum PF of ∼1.0 μW/K^2·cm was calculated at ∼293 and ∼533 K.

Furthermore, in-plane κ measurement (Figure 6a) shows the values to be in the range of 4.5−5.5 W/m·K in the ∼293−533 K temperature range.[56,58] The TE figure of merit, zT (zT = PF·T/κ), is used to assess a material's TE performance, where PF and T are the power factor and the absolute temperature, respectively. zT is calculated based on the obtained PF and κ results as illustrated in Figure 6b. It follows a similar trend to the PF, reaching a maximum zT of ∼0.01 at 533 K.

3.3. Performance Analysis of Chalcogenides/AZO TEGs. V_{OC} vs ΔT measurements give information on the maximum voltage that can be generated by the fabricated chalcogenides/AZO thin-film TEGs at specific ΔTs. A hotplate was used to control T_h with a 10 K increment from ∼323 K up to ∼523 K, while T_c was kept at ambient temperature with a metal plate as the heat sink. The measured ΔTs did not fully match the set temperature of T_h and T_c due to substrate buffer and poor heat sink setup. Substrate buffer may affect the efficiency of the TEG, as some of the temperature gradients will be lost across the substrate.[59]

Figure 7 shows the V_{OC} vs ΔT plot of chalcogenides/AZO thin-film TEGs, presenting a linear trend of voltage with ΔT. Maximum voltages measured for TEGs with HI CZTS, BM CZTSe, BM CZTSSe, and BM CTS *p*-legs at ΔT 160 K were ∼87, ∼118, ∼46, and ∼98 mV, respectively. Since AZO is a constant throughout the TEGs, these values are directly related to the α of the chalcogenides around 480−500 K, as shown in Figure 4a, where BM CZTSe possesses the highest value, followed by CTS, HI CZTS, and BM CZTSSe. The selected temperature range corresponds to the temperature taken by the thermal camera at the TEG's hot side. However, a thorough relation between V_{OC} and α is yet to be explored.

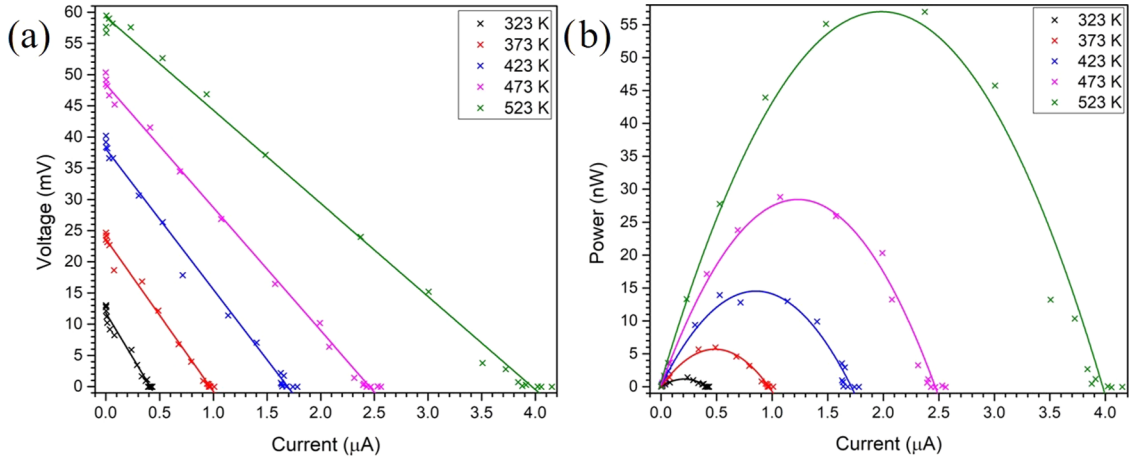

Figure 8. (a) *I*−*V* and (b) *I*−*P* plots of thin-film HI CZTS/AZO thin-film TEG at different ΔTs.

https://doi.org/10.1021/acsaem.2c00268
ACS Appl. Energy Mater. 2022, 5, 5909−5918

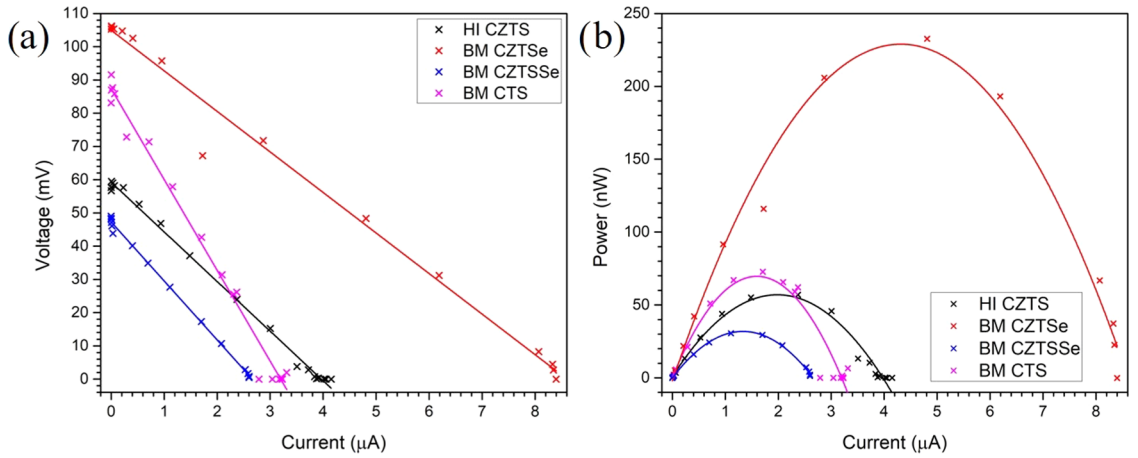

Figure 9. (a) $I-V$ and (b) $I-P$ plots of chalcogenides/AZO thin-film TEGs.

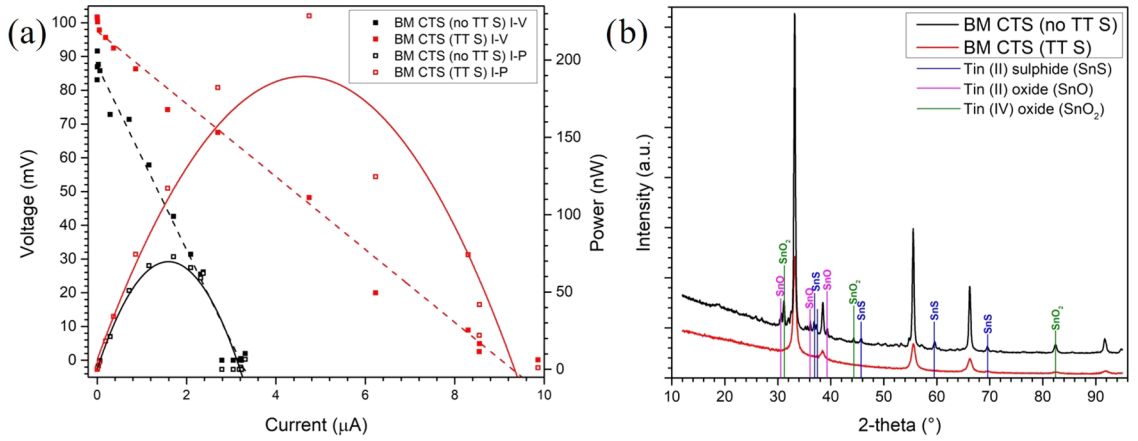

Figure 10. (a) $I-V-P$ plots and (b) XRD patterns of sulfurized and nonsulfurized BM CTS/AZO thin-film TEG.

Figure 8 shows the $I-V-P$ measurements of HI CZTS/AZO thin-film TEG at different ΔTs. For simplicity, the figures were separated into $I-V$ (Figure 8a) and $I-P$ (Figure 8b) plots. The temperatures indicate the hotplate temperature that was set on the T_h side of the TEG, since it is the main component in determining ΔT, as discussed before. The $I-V$ plots are linear for all of the ΔTs, with the slope of the plots indicating the TEG's internal resistance. The values of the slopes reduced from 28.6 kΩ at 323 K to 14.9 kΩ at 523 K, which agrees with the reduction of CZTS resistivity at elevated temperatures, as previously discussed and with the approximately constant trend of resistivity for AZO, neglecting the small resistivity effect of Ag metal contacts.[60] On the other hand, the $I-P$ curve shows the classical parabolic shape, with maximum power occurring at the point where the load resistance matches the device resistance.[48] The results show that a higher ΔT produces a higher power output, which reaches up to ∼55 nW at 523 K T_h.

In addition to HI CZTS thin-film TEG, internal resistances of the other chalcogenide/AZO thin-film TEGs were also obtained from the slopes of their respective $I-V$ plots. At similar T_h of 523 K and ΔT of 160 K, Figure 9a shows that the chalcogenide/AZO thin-film TEG with BM CZTSe p-legs possesses the lowest internal resistance (12.2 kΩ), followed by HI CZTS (14.9 kΩ), BM CZTSSe (17.7 kΩ), and BM CTS (27.3 kΩ). The internal resistance may be affected by factors including but not limited to the deposited films' thicknesses and materials' resistivities, such as carrier concentrations and carrier mobilities. In addition, low film density may also result in low carrier mobility. This leads to a smaller effective area of conduction, poorer connectivity of domains, and carrier scattering (decreasing carrier mean free path), thus providing a major obstacle for electrical conduction.[61]

The $I-V$ plot in Figure 9b reveals that the TEG with BM CZTSe p-legs performs the best with maximum power output reaching ∼240 nW, followed by BM CTS (∼75 nW), HI CZTS (∼55 nW), and BM CZTSSe (∼30 nW). From the results obtained, the calculated maximum power output per unit active planar area for each TEG is ∼188, ∼59, ∼43, and ∼23 nW/cm^2, respectively. The exceptional performance of BM CZTSe is evident from its high V_{OC} and low internal resistance compared to the other chalcogenides. From the obtained results, we can deduce that a TEG's performance is significantly affected by two main factors: (1) V_{OC}, which is directly related to α, and (2) internal resistance, which is directly related to the film thickness and density and ρ.

In addition, the fabricated TEGs also showed a significant performance improvement as compared to other thin-film TEGs using low-cost and abundant materials such as tin oxide/zinc oxide (SnO_x/ZnO)[62] and aluminum oxide/zinc oxide (Al_2O_3/ZnO),[48] which only generated maximum power output per unit active planar area of ∼2.8 nW/cm^2 at ΔT 160 K and ∼1.6 nW/cm^2 at ΔT 80 K, respectively. From this comparison, it can be surmised that this work successfully

https://doi.org/10.1021/acsaem.2c00268
ACS Appl. Energy Mater. 2022, 5, 5909−5918

established a fabrication method of high-performing thin-film TEGs using a facile, low-cost, and scalable approach. However, the TEG performance was still low as compared to TEGs with conventional materials such as bismuth telluride (Bi_2Te_3)[63] and antimony telluride (Sb_2Te_3),[64] which respectively produced maximum power per unit active planar area of ~955 nW/cm^2 at ΔT 20 K and ~305 nW/cm^2 at ΔT 15 K. Nevertheless, the fabricated *p*-type chalcogenides may provide insights for future studies to replace the scarce, expensive, and potentially harmful elements used in the current conventional materials.

3.4. Effect of Sulfurization. In a different sample of BM CTS/AZO TEG, the CTS was subjected to a second thermal treatment with the same procedure as the first, but with the addition of an excess amount of S. As shown in Figure 10a, the TEG with sulfurized CTS performs significantly better compared to that with nonsulfurized CTS with a maximum power output of ~230 nW, which is a staggering 300% increase in performance. This BM CTS/AZO TEG provides an alternative for chalcogenide/AZO TEGs with a much safer stoichiometry, which is Se-free.

The main reason for this improvement can be attributed to the suppression of spurious phases, as visible in the XRD patterns of Figure 10b, including tin(II) oxide (SnO), tin(IV) oxide (SnO_2), and tin(II) sulfide (SnS), which were formed due to loss of S.[65] Even though SnS possesses comparable transport properties to CTS, tin oxides, on the other hand, have much poorer transport properties (particularly SnO_2, with *n*-type behavior),[66] which detrimentally affects the TEG's performance. In addition, sulfurization also improves the CTS electrical properties by assisting the formation of void-free CTS films,[67] as can be seen by reduced internal resistance from 27.3 to 10.8 kΩ from the slope of *I*−*V* curve, which in turn enhances the TEG's performance.

4. CONCLUSIONS AND OUTLOOK

This work presented a complete fabrication method of thin-film TEGs using Cu/Zn/Sn-based ternary and quaternary chalcogenide *p*-legs and AZO *n*-legs. Chalcogenide thin films were deposited by spin-coating using chalcogenide inks synthesized either through hot injection or ball-milling, while AZO was deposited by sputtering. Several factors that affect the performance of the fabricated TEGs, including the composition, TEGs' internal resistance, V_{OC}, and sulfurization, have been thoroughly discussed. The devices are suitable for medium- to high-temperature TE applications with CZTSe/AZO TEG as the champion device, showing the maximum power output of ~240 nW at ΔT 160 K (T_h ~483 K, T_c ~323 K). These fabricated TEGs showed a significant performance improvement for a thin-film TEG as compared to other thin-film TEGs using abundant, low-cost, and safer materials, which only show nanowatts[48,68] of power output. These chalcogenide/AZO TEGs may provide alternatives or insights into replacing scarce, expensive, and potentially harmful elements used in TE materials such as antimony (Sb),[44] tellurium (Te),[23,63] lead (Pb),[22,46] bismuth (Bi),[8,63] and germanium (Ge).[69] In conclusion, this work managed to demonstrate the fabrication of a working thin-film TEG using abundant and safer materials with a facile, low-cost, and scalable approach. Further studies are warranted to better understand and improve the performance of the individual components in the chalcogenides/AZO TEG. Several suggestions from the authors include the studies on film thickness and density improvement, thickness optimization, effects of doping, and device stability. Future work will also involve the investigation of alternative chalcogenide *n*-leg materials in the spirit of fabricating a fully optimized, nontoxic, and low-cost device.

■ ASSOCIATED CONTENT

Supporting Information

The Supporting Information is available free of charge at https://pubs.acs.org/doi/10.1021/acsaem.2c00268.

Synthesis of Cu−Zn−Sn chalcogenides, dynamic light scattering (DLS) analysis, deposition of thin-film chalcogenides, deposition of AZO *n*-legs and Ag metal contacts in TEG fabrication, thin-film characterization, chalcogenides/AZO thin-film TEGs performance analysis, preliminary characterization of hot-injection (HI) CZTS thin films, preliminary characterization of Cu−Zn−Sn chalcogenide thin films, characterization of AZO thin film, and TE transport properties of HI CZTS thin film (PDF)

■ AUTHOR INFORMATION

Corresponding Authors

Ubaidah Syafiq − *Department of Civil, Environmental and Mechanical Engineering, University of Trento, Trento 38123 TN, Italy; Solar Energy Research Institute, the National University of Malaysia (SERI-UKM), 43600 Bangi, Selangor, Malaysia;* orcid.org/0000-0002-0167-9495; Email: ubaidahsyafiq@ukm.edu.my

Paolo Scardi − *Department of Civil, Environmental and Mechanical Engineering, University of Trento, Trento 38123 TN, Italy;* orcid.org/0000-0003-1097-3917; Email: paolo.scardi@unitn.it

Authors

Eleonora Isotta − *Department of Civil, Environmental and Mechanical Engineering, University of Trento, Trento 38123 TN, Italy;* orcid.org/0000-0002-5864-463X

Narges Ataollahi − *Department of Civil, Environmental and Mechanical Engineering, University of Trento, Trento 38123 TN, Italy;* orcid.org/0000-0002-8135-6054

Ketan Lohani − *Department of Civil, Environmental and Mechanical Engineering, University of Trento, Trento 38123 TN, Italy;* orcid.org/0000-0003-1059-6744

Sally Luong − *School of Engineering and Materials Science, Queen Mary University of London, London E1 4NS, U.K.*

Vanira Trifiletti − *School of Engineering and Materials Science, Queen Mary University of London, London E1 4NS, U.K.; Department of Materials Science, University of Milano-Bicocca, Milan 20125 MI, Italy*

Oliver Fenwick − *School of Engineering and Materials Science, Queen Mary University of London, London E1 4NS, U.K.;* orcid.org/0000-0001-7499-5117

Complete contact information is available at: https://pubs.acs.org/10.1021/acsaem.2c00268

Notes

The authors declare no competing financial interest.

■ REFERENCES

(1) Strohl, G. R.; Harpster, J. W. Thermoelectric Power Generator - Principles of Operation. https://www.britannica.com/technology/

thermoelectric-power-generator/Principles-ofoperation (accessed July 1, 2021).
(2) Bell, L. E. Cooling, Heating, Generating Power, and Recovering Waste Heat with Thermoelectric Systems. *Science* **2008**, *321*, 1457−1461.
(3) Chen, A.; Wright, P. K. Medical Applications of Thermoelectrics. In *Modules, Systems, and Applications in Thermoelectrics*; CRC Press, 2012; pp 535−564.
(4) Min, G.; Rowe, D. M. Cooling Performance of Integrated Thermoelectric Microcooler. *Solid-State Electron.* **1999**, *43*, 923−929.
(5) Disalvo, F. J. Thermoelectric Cooling and Power Generation. *Science* **1999**, *285*, 703−706.
(6) Fan, P.; Zheng, Z. H.; Li, Y. Z.; Lin, Q. Y.; Luo, J. T.; Liang, G. X.; Cai, X. M.; Zhang, D. P.; Ye, F. Low-Cost Flexible Thin Film Thermoelectric Generator on Zinc Based Thermoelectric Materials. *Appl. Phys. Lett.* **2015**, *106*, No. 073901.
(7) Hicks, L. D.; Dresselhaus, M. S. Effect of Quantum-Well Structures on the Thermoelectric Figure of Merit. *Phys. Rev. B: Condens. Matter Mater. Phys.* **1993**, *47*, 12727−12731.
(8) Venkatasubramanian, R.; Siivola, E.; Colpitts, T.; O'Quinn, B. Thin-Film Thermoelectric Devices with High Room-Temperature Figures of Merit. *Nature* **2001**, *413*, 597−602.
(9) Dresselhaus, M. S.; Chen, G.; Tang, M. Y.; Yang, R.; Lee, H.; Wang, D.; Ren, Z.; Fleurial, J. P.; Gogna, P. New Directions for Low-Dimensional Thermoelectric Materials. *Adv. Mater.* **2007**, *19*, 1043−1053.
(10) Chen, X.; Zhou, Z.; Lin, Y. H.; Nan, C. Thermoelectric Thin Films: Promising Strategies and Related Mechanism on Boosting Energy Conversion Performance. *J. Materiomics* **2020**, *6*, 494−512.
(11) Li, J. F.; Liu, W. S.; Zhao, L. D.; Zhou, M. High-Performance Nanostructured Thermoelectric Materials. *NPG Asia Mater.* **2010**, *2*, 152−158.
(12) Szczech, J. R.; Higgins, J. M.; Jin, S. Enhancement of the Thermoelectric Properties in Nanoscale and Nanostructured Materials. *J. Mater. Chem.* **2011**, *21*, 4037−4055.
(13) White, M. A.; Medina-Gonzalez, A. M.; Vela, J. Soft Chemistry, Coloring and Polytypism in Filled Tetrahedral Semiconductors: Toward Enhanced Thermoelectric and Battery Materials. *Chem. - Eur. J.* **2018**, *24*, 3650−3658.
(14) Kim, S. J.; We, J. H.; Cho, B. J. A Wearable Thermoelectric Generator Fabricated on a Glass Fabric. *Energy Environ. Sci.* **2014**, *7*, 1959−1965.
(15) Park, N. W.; Park, T. H.; Ahn, J. Y.; Kang, S. H.; Lee, W. Y.; Yoon, Y. G.; Yoon, S. G.; Lee, S. K. Thermoelectric Characterization and Fabrication of Nanostructured P-Type Bi0.5Sb1.5Te3 and n-Type Bi2Te3 Thin Film Thermoelectric Energy Generator with an in-Plane Planar Structure. *AIP Adv.* **2016**, *6*, No. 065123.
(16) Chen, W. Y.; Shi, X. L.; Zou, J.; Chen, Z. G. Thermoelectric Coolers: Progress, Challenges, and Opportunities. *Small Methods* **2022**, *6*, No. 2101235.
(17) Kim, M.-Y.; Oh, T.-S. Thermoelectric Characteristics of the Thermopile Sensors with Variations of the Width and the Thickness of the Electrodeposited Bismuth-Telluride and Antimony-Telluride Thin Films. *Mater. Trans.* **2010**, *51*, 1909−1913.
(18) Parveen, S.; Victor Vedanayakam, S.; Padma Suvarna, R. Thermoelectric Generator Electrical Performance Based on Temperature of Thermoelectric Materials. *Int. J. Eng. Technol.* **2018**, *7*, 189.
(19) Isotta, E.; Syafiq, U.; Ataollahi, N.; Chiappini, A.; Malerba, C.; Luong, S.; Trifiletti, V.; Fenwick, O.; Pugno, N.; Scardi, P. Thermoelectric Properties of CZTS Thin Films: Effect of Cu-Zn Disorder. *Phys. Chem. Chem. Phys.* **2021**, *23*, 13148−13158.
(20) Shi, X. L.; Chen, W. Y.; Zhang, T.; Zou, J.; Chen, Z. G. Fiber-Based Thermoelectrics for Solid, Portable, and Wearable Electronics. *Energy Environ. Sci.* **2021**, *14*, 729−764.
(21) Cao, T.; Shi, X.-L.; Zou, J.; Chen, Z.-G. Advances in Conducting Polymer-Based Thermoelectric Materials and Devices. *Microstructures* **2021**, DOI: 10.20517/microstructures.2021.06.
(22) Biswas, K.; He, J.; Blum, I. D.; Wu, C. I.; Hogan, T. P.; Seidman, D. N.; Dravid, V. P.; Kanatzidis, M. G. High-Performance Bulk Thermoelectrics with All-Scale Hierarchical Architectures. *Nature* **2012**, *489*, 414−418.
(23) Bao, D.; Sun, Q.; Huang, L.; Chen, J.; Tang, J.; Zhou, D.; Hong, M.; Yang, L.; Chen, Z. G. Thermoelectric Performance of P-Type (Bi,Sb)2Te3 Incorporating Amorphous Sb2S3 Nanospheres. *Chem. Eng. J.* **2022**, *430*, No. 132738.
(24) Meng, H.; An, M.; Luo, T.; Yang, N. Thermoelectric Applications of Chalcogenides. In *Chalcogenide: From 3D to 2D and Beyond*; Liu, X.; Lee, S.; Furdyna, J. K.; Luo, T.; Zhang, Y.-H., Eds.; Woodhead Publishing: Duxford, 2020; Vol. *42*, pp 31−56.
(25) Zhao, L. D.; Lo, S. H.; Zhang, Y.; Sun, H.; Tan, G.; Uher, C.; Wolverton, C.; Dravid, V. P.; Kanatzidis, M. G. Ultralow Thermal Conductivity and High Thermoelectric Figure of Merit in SnSe Crystals. *Nature* **2014**, *508*, 373−377.
(26) Isotta, E.; Pugno, N. M.; Scardi, P. Nanostructured Kesterite (Cu2ZnSnS4) for Applications in Thermoelectric Devices. *Powder Diffr.* **2019**, *34*, 1−6.
(27) Isotta, E.; Fanciulli, C.; Pugno, N. M.; Scardi, P. Effect of the Order-Disorder Transition on the Seebeck Coefficient of Nanostructured Thermoelectric Cu2ZnSnS4. *Nanomaterials* **2019**, *9*, 762.
(28) Isotta, E.; Mukherjee, B.; Fanciulli, C.; Pugno, N. M.; Scardi, P. Order-Disorder Transition in Kesterite Cu2ZnSnS4: Thermopower Enhancement via Electronic Band Structure Modification. *J. Phys. Chem. C* **2020**, *124*, 7091−7096.
(29) Jiang, Q.; Yan, H.; Lin, Y.; Shen, Y.; Yang, J.; Reece, M. J. Colossal Thermoelectric Enhancement in Cu2+xZn1−xSnS4solid Solution by Local Disordering of Crystal Lattice and Multi-Scale Defect Engineering. *J. Mater. Chem. A* **2020**, *8*, 10909−10916.
(30) Isotta, E.; Mukherjee, B.; Fanciulli, C.; Ataollahi, N.; Sergueev, I.; Stankov, S.; Edla, R.; Pugno, N. M.; Scardi, P. Origin of a Simultaneous Suppression of Thermal Conductivity and Increase of Electrical Conductivity and Seebeck Coefficient in Disordered Cubic Cu2ZnSnS4. *Phys. Rev. Appl.* **2020**, *14*, No. 064073.
(31) Lohani, K.; Isotta, E.; Ataollahi, N.; Fanciulli, C.; Chiappini, A.; Scardi, P. Ultra-Low Thermal Conductivity and Improved Thermoelectric Performance in Disordered Nanostructured Copper Tin Sulphide (Cu2SnS3, CTS). *J. Alloys Compd.* **2020**, *830*, No. 154604.
(32) Lohani, K.; Nautiyal, H.; Ataollahi, N.; Fanciulli, C.; Sergueev, I.; Etter, M.; Scardi, P. Experimental and Ab Initio Study of Cu2SnS3 (CTS) Polymorphs for Thermoelectric Applications. *J. Phys. Chem. C* **2021**, *125*, 178−188.
(33) Lohani, K.; Nautiyal, H.; Ataollahi, N.; Maji, K.; Guilmeau, E.; Scardi, P. Effects of Grain Size on the Thermoelectric Properties of Cu2SnS3: An Experimental and First-Principles Study. *ACS Appl. Energy Mater.* **2021**, *4*, 12604−12612.
(34) Syafiq, U.; Ataollahi, N.; Scardi, P. Progress in CZTS as Hole Transport Layer in Perovskite Solar Cell. *Sol. Energy* **2020**, *196*, 399−408.
(35) Syafiq, U.; Ataollahi, N.; Maggio, R. di.; Scardi, P. Solution-Based Synthesis and Characterization of Cu2ZnSnS4 (CZTS) Thin Films. *Molecules* **2019**, *24*, 3454.
(36) Kush, P.; Deka, S. Multifunctional Copper-Based Quaternary Chalcogenide Semiconductors Toward State-of-the-Art Energy Applications. *ChemNanoMat* **2019**, *5*, 373−402.
(37) Jo, E.; Gang, M. G.; Shim, H.; Suryawanshi, M. P.; Ghorpade, Uv.; Kim, J. H. 8% Efficiency Cu2ZnSn(S,Se)4 (CZTSSe) Thin Film Solar Cells on Flexible and Lightweight Molybdenum Foil Substrates. *ACS Appl. Mater. Interfaces* **2019**, *11*, 23118−23124.
(38) Gunavathy, K. V.; Tamilarasan, K.; Rangasami, C.; Arulanantham, A. M. S. Solution Processed Copper Zinc Tin Sulfide Thin Films for Thermoelectric Device Applications. *Ceram. Int.* **2020**, *46*, 28342−28354.
(39) Zeng, Y.; Liang, G.; Fan, P.; Xie, Y.; Fan, B.; Hu, J.; Zheng, Z.; Zhang, X.; Luo, J.; Zhang, D. The Structural, Optical and Thermoelectric Properties of Single Target Sputtered Cu2ZnSn-(S,Se)4 Thin Film. *J. Mater. Sci.: Mater. Electron.* **2017**, *28*, 13763−13769.
(40) Liu, M. L.; Huang, F. Q.; Chen, L. D.; Chen, I. W. A Wide-Band-Gap p-Type Thermoelectric Material Based on Quaternary

Chalcogenides of Cu2ZnSnQ4 (Q=S,Se). *Appl. Phys. Lett.* **2009**, *94*, No. 202103.
(41) Baranowski, L. L.; McLaughlin, K.; Zawadzki, P.; Lany, S.; Norman, A.; Hempel, H.; Eichberger, R.; Unold, T.; Toberer, E. S.; Zakutayev, A. Effects of Disorder on Carrier Transport in Cu2SnS3. *Phys. Rev. Appl.* **2015**, *4*, No. 044017.
(42) Guo, H.; Wang, S.; Wang, L.; Jin, K.; Chen, S.; Fu, G.; Ge, C.; Lu, H.; Wang, C.; He, M.; Yang, G. Electrical Properties of Thermoelectric Cobalt Ca3Co4O9 Epitaxial Heterostructures. *J. Appl. Phys.* **2013**, *113*, No. 113707.
(43) Aabdin, Z.; Peranio, N.; Winkler, M.; Bessas, D.; König, J.; Hermann, R. P.; Böttner, H.; Eibl, O. Sb2Te3 and Bi2Te3 Thin Films Grown by Room-Temperature MBE. *J. Electron. Mater.* **2011**, *41*, 1493−1497.
(44) Takayama, K.; Takashiri, M. Multi-Layered-Stack Thermoelectric Generators Using p-Type Sb2Te3 and n-Type Bi2Te3 Thin Films by Radio-Frequency Magnetron Sputtering. *Vacuum* **2017**, *144*, 164−171.
(45) Lu, Z.; Layani, M.; Zhao, X.; Tan, L. P.; Sun, T.; Fan, S.; Yan, Q.; Magdassi, S.; Hng, H. H. Fabrication of Flexible Thermoelectric Thin Film Devices by Inkjet Printing. *Small* **2014**, *10*, 3551−3554.
(46) Harman, T. C.; Taylor, P. J.; Walsh, M. P.; LaForge, B. E. Quantum Dot Superlattice Thermoelectric Materials and Devices. *Science* **2002**, *297*, 2229−2232.
(47) Heo, S. H.; Jo, S.; Kim, H. S.; Choi, G.; Song, J. Y.; Kang, J. Y.; Park, N. J.; Ban, H. W.; Kim, F.; Jeong, H.; Jung, J.; Jang, J.; Lee, W. B.; Shin, H.; Son, J. S. Composition Change-Driven Texturing and Doping in Solution-Processed SnSe Thermoelectric Thin Films. *Nat. Commun.* **2019**, *10*, No. 864.
(48) Park, N. W.; Ahn, J. Y.; Park, T. H.; Lee, J. H.; Lee, W. Y.; Cho, K.; Yoon, Y. G.; Choi, C. J.; Park, J. S.; Lee, S. K. Control of Phonon Transport by the Formation of the Al2O3 Interlayer in Al2O3-ZnO Superlattice Thin Films and Their in-Plane Thermoelectric Energy Generator Performance. *Nanoscale* **2017**, *9*, 7027−7036.
(49) Syafiq, U.; Ataollahi, N.; DiMaggio, R.; Scardi, P. Solution-Based Synthesis and Characterization Ofcu2znsns4 (Czts) Thin Films. *Molecules* **2019**, *24*, No. 3454.
(50) Ataollahi, N.; Bazerla, F.; Malerba, C.; Chiappini, A.; Ferrari, M.; Maggio, R.; Di Scardi, P. Synthesis and Post-Annealing of Cu 2 ZnSnS 4 Absorber Layers Based on Oleylamine / 1-Dodecanethiol. *Materials* **2019**, *12*, No. 3320.
(51) Ternero, F.; Rosa, L. G.; Urban, P.; Montes, J. M.; Cuevas, F. G. Influence of the Total Porosity on the Properties of Sintered Materials—A Review. *Metals* **2021**, *11*, 730.
(52) Khanna, V. K. Temperature Effects on Semiconductors. In *Extreme-Temperature and Harsh-Environment Electronics: Physics, Technology and Applications*; Khanna, V. K., Ed.; IOP Publishing: Bristol, 2017; pp 3-1−3-33.
(53) Scragg, J. J. S.; Choubrac, L.; Lafond, A.; Ericson, T.; Platzer-Björkman, C. A Low-Temperature Order-Disorder Transition in Cu2ZnSnS4 Thin Films. *Appl. Phys. Lett.* **2014**, *104*, No. 041911.
(54) Seebeck, T. J. Ueber Die Magnetische Polarisation Der Metalle Und Erze Durch Temperatur-Differenz. *Ann. Phys.* **1826**, *82*, 133−160.
(55) Abutaha, A. I.; Sarath Kumar, S. R.; Alshareef, H. N. Crystal Orientation Dependent Thermoelectric Properties of Highly Oriented Aluminum-Doped Zinc Oxide Thin Films. *Appl. Phys. Lett.* **2013**, *102*, No. 053507.
(56) Jantrasee, S.; Moontragoon, P.; Pinitsoontorn, S. Thermoelectric Properties of Al-Doped ZnO: Experiment and Simulation. *J. Semicond.* **2016**, *37*, No. 092002.
(57) Chen, T. H.; Cheng, T. C.; Hu, Z. R. The Electrical and Optical Properties of AZO Thin Film under Different Post-Annealing Temperatures. *Microsyst. Technol.* **2013**, *19*, 1787−1790.
(58) Jood, P.; Mehta, R. J.; Zhang, Y.; Peleckis, G.; Wang, X.; Siegel, R. W.; Borca-Tasciuc, T.; Dou, S. X.; Ramanath, G. Al-Doped Zinc Oxide Nanocomposites with Enhanced Thermoelectric Properties. *Nano Lett.* **2011**, *11*, 4337−4342.
(59) *Energy Harvesting Technologies*; Priya, S.; Inman, D. J., Eds.; Springer Science+Business Media, LLC: New York, 2009.
(60) De Vries, J. W. C. Temperature and Thickness Dependence of the Resistivity of Thin Polycrystalline Aluminium, Cobalt, Nickel, Palladium, Silver and Gold Films. *Thin Solid Films* **1988**, *167*, 25−32.
(61) Choi, S. K.; Lee, J. I. Effect of Film Density on Electrical Properties of Indium Tin Oxide Films Deposited by Dc Magnetron Reactive Sputtering. *J. Vac. Sci. Technol., A* **2001**, *19*, 2043−2047.
(62) Vieira, E. M. F.; Silva, J. P. B.; Veltruská, K.; Istrate, C. M.; Lenzi, V.; Trifiletti, V.; Lorenzi, B.; Matolín, V.; Ghica, C.; Marques, L.; Fenwick, O.; Goncalves, L. M. All-Oxide p-n Junction Thermoelectric Generator Based on SnOx and ZnO Thin Films. *ACS Appl. Mater. Interfaces* **2021**, *13*, 35187−35196.
(63) Ding, D.; Sun, F.; Xia, F.; Tang, Z. A High-Performance and Flexible Thermoelectric Generator Based on the Solution-Processed Composites of Reduced Graphene Oxide Nanosheets and Bismuth Telluride Nanoplates. *Nanoscale Adv.* **2020**, *2*, 3244−3251.
(64) Yamamuro, H.; Takashiri, M. Power Generation in Slope-Type Thin-Film Thermoelectric Generators by the Simple Contact of a Heat Source. *Coatings* **2019**, *9*, No. 63.
(65) Ashfaq, A.; Jacob, J.; Mahmood, K.; Mehboob, K.; Ikram, S.; Ali, A.; Amin, N.; Hussain, S.; Rehman, U. Effect of Sulfur Amount during Post-Growth Sulfurization Process on the Structural, Morphological and Thermoelectric Properties of Sol-Gel Grown Quaternary Chalcogenide Cu2ZnSnS4 Thin Films. *Phys. B* **2021**, *602*, No. 412497.
(66) Solola, G. T.; Klopov, M.; Akinami, J. O.; Afolabi, T. A.; Zh Karazhanov, S.; Adebayo, G. First Principle Calculations of Structural, Electronic, Optical and Thermoelectric Properties of Tin (II) Oxide. *Mater. Res. Express* **2019**, *6*, No. 125915.
(67) Zhao, Y.; Han, X.; Xu, B.; Dong, C.; Li, J.; Yan, X. Effect of Sulfurization Process on the Properties of Solution-Processed Cu2SnS3 Thin Film Solar Cells. *J. Mater. Sci.: Mater. Electron.* **2019**, *30*, 17947−17955.
(68) Burton, M. R.; Liu, T.; McGettrick, J.; Mehraban, S.; Baker, J.; Pockett, A.; Watson, T.; Fenwick, O.; Carnie, M. J. Thin Film Tin Selenide (SnSe) Thermoelectric Generators Exhibiting Ultralow Thermal Conductivity. *Adv. Mater.* **2018**, *30*, No. 1801357.
(69) Li, Y.; Wang, G.; Akbari-Saatlu, M.; Procek, M.; Radamson, H. H. Si and SiGe Nanowire for Micro-Thermoelectric Generator: A Review of the Current State of the Art. *Front. Mater.* **2021**, *8*, No. 78.

https://doi.org/10.1021/acsaem.2c00268
ACS Appl. Energy Mater. 2022, 5, 5909−5918